Accepted Manuscript

Evaluating the textural and mechanical properties of an Mg-Dy alloy processed by high-pressure torsion

Abdelkader Hanna, Hiba Azzeddine, Rabeb Lachhab, Thierry Baudin, Anne-Laure Helbert, François Brisset, Yi Huang, Djamel Bradai, Terence G. Langdon

Please cite this article as: A. Hanna, H. Azzeddine, R. Lachhab, T. Baudin, A.-L. Helbert, Franç. Brisset, Y. Huang, D. Bradai, T.G. Langdon, Evaluating the textural and mechanical properties of an Mg-Dy alloy processed by high-pressure torsion, *Journal of Alloys and Compounds* (2018), doi: https://doi.org/10.1016/j.jallcom.2018.11.109.

Evaluating the textural and mechanical properties of an Mg-Dy alloy

processed by high-pressure torsion

Abdelkader Hanna[a,b], Hiba Azzeddine[b,c*], Rabeb Lachhab[d], Thierry Baudin[e],

Anne-Laure Helbert[e], François Brisset[e], Yi Huang[f,g], Djamel Bradai[c], Terence G. Langdon[f]

[a] Physics and Chemistry of Materials Laboratory, Department of Physics, University Mohamed Boudiaf, M'sila, 28000, Algeria
[b] University Mohamed Boudiaf, M'sila, 28000,Algeria.
[c] Faculty of Physics, USTHB, Algiers, Algeria.
[d] Laboratoire de Chimie Inorganique Ur-11-Es-73, Faculté des Sciences Sfax, BP 1171, 3018, Sfax Tunisia.
[e] ICMMO, SP2M, Univ. Paris-Sud, Université Paris-Saclay, UMR CNRS 8182, 91405 Orsay Cedex, France
[f] Materials Research Group, Department of Mechanical Engineering, University of Southampton, Southampton SO17 1BJ, UK
[g] Department of Design and Engineering, Faculty of Science and Technology, Bournemouth University, Poole, Dorset BH12 5BB, UK
[*] Corresponding author: azehibou@yahoo.fr

Abstract

Samples of an Mg-0.41Dy (wt. %) alloy were severely deformed by high-pressure torsion (HPT) at room temperature up to 15 turns and the texture, microstructure and microhardness values in the centres, mid-radial points and edges of the HPT-deformed discs were investigated using X-ray diffraction, Electron BackScatter Diffraction and Vickers microhardness measurements. The textures in the centres of discs were characterized by a typical weak basal fiber whereas at both the mid-points and edges of the discs there was a strong basal texture where the c-axis of most grains was shifted 15° away from the shear direction. An almost homogeneous ultrafine-grained structure with a grain size of about 0.75 µm was achieved after 15 HPT turns. The microhardness values in these three positions increased with increasing numbers of turns, reached a maximum and then decreased to a lower steady-state level at large strains. In addition to dislocation and grain size hardening, the results show that texture strengthening contributes significantly to the rapid increase in hardening in the early stages of deformation.

Keywords: Hardening; High-Pressure Torsion; Mg-Dy alloy; Microhardness; Texture

1. Introduction

Rare earth (RE) magnesium (Mg-RE) alloys have received special attention over the last few years because of their attractive mechanical properties at both ambient and elevated temperatures combined with their high specific strength, good creep resistance and excellent castability [1, 2]. It was reported that Mg-RE alloys exhibit more isotropic behavior under deformation than conventional Mg-based alloys such as the AZ31 (Mg-3Al-1Zn, wt.%) alloy [3] where these improvements are achieved through texture weakening [1]. Various mechanisms have been proposed to explain the precise influence of the RE elements including a Particle-Stimulated Nucleation (PSN) mechanism [4], an enhancement of shear banding [5], an activation of non-basal slip systems [6], an oriented growth of recrystallized grain nuclei [7] and effects due to the grain boundary energy and mobility [8].

Despite this considerable attention, the use of commercial Mg alloys containing heavy additions of RE elements, such as the Mg-Y-Rare Earth (WE series), is essentially limited to products for the aerospace and aircraft sectors because of the high costs. Several possible strategies have been proposed to develop new Mg-RE alloys having higher strength and lower cost where most of this research was focused on determining the level of low price RE (Y, La, Ce, Nd) alloying elements that are required to modify the texture and unravel their role during deformation and recrystallization processes [9, 10]. From this approach, it was demonstrated that a texture weakening may occur due to RE elements at alloying concentrations as low as 0.1 wt.% (~0.02 at.%) [11].

It is now well-established that conventional thermo-mechanical processing, such as hot extrusion and hot rolling, leads to substantial grain refinement, improves the mechanical properties and insures a good thermal stability of the Mg-RE based alloys [12, 13]. Furthermore, the severe plastic deformation (SPD) process of high-pressure torsion (HPT) is generally considered the most effective procedure for achieving exceptional grain refinement,

typically to the submicrometer or nanometer ranges, in Mg-based alloys at room temperature [14, 15]. Grain refinement is successful without cracking in HPT processing due to the imposed hydrostatic pressure which effectively prevents propagation of fracture during the torsional straining [16]. Several reports are now available describing the application of HPT to pure Mg and Mg-based alloys with the production of average grain sizes down to the nanoscale [14–21]. Some new Mg alloys with high content of RE elements have also been successfully processed by HPT at room temperature [15, 22–27]. For example, the average grain size of an Mg-8.2Gd-3.8Y-1.0Zn-0.4Zr (wt.%) alloy decreased from ~85 μm in the as-cast condition to ~55 nm after HPT processing up to16 turns [22] and an Mg–9Gd–4Y–0.4Zr (wt.%) alloy with an initial grain size of ~ 8.6 μm was processed by HPT at room temperature to produce refined grains of ~85 nm after 16 turns and superplastic behavior [24]. Similar grain refinement and superplasticity was reported also in a binary Mg-10Gd (wt.%) alloy processed by HPT [28]. Nevertheless, there has been no critical investigation of the texture and microstructural evolution during SPD processing and no comprehensive analysis is available determining the significance of the various strengthening mechanisms in Mg-RE alloys.

The present research was initiated in order to address this deficiency. Specifically, a binary Mg-0.41Dy (wt. %) alloy was processed by HPT, the mechanical properties were recorded after processing and the evolution of the microstructure and texture were evaluated to permit an analysis of the relevant strengthening mechanisms.

2. Experimental material and procedures

The Mg-0.41Dy (wt.%) alloy was supplied in an as-cast state by Dr. Talal Al-Samman from the Institute für Metallkunde und Metallphysik (IMM-RWTH) in Aachen, Germany. An examination showed that the microstructure of the as-cast Mg-0.41Dy was very coarse and

elongated with an average grain size larger than ~2 mm (Figure 1) and exhibits a random texture (not shown).

Discs with diameters of 10 mm and thicknesses of 1.5 mm were machined from the as-cast material and then carefully polished with abrasive papers to final thicknesses of ~0.9 mm. The HPT processing was conducted at room temperature with a rotational speed of 1 rpm through 1/4, 1/2, 1, 5, 10 and 15 turns using an imposed applied pressure of 6.0 GPa. All discs were processed under quasi-constrained conditions [29, 30] where there is a limited outward flow of material around the periphery of the disc during the processing operation. Figure 2 provides a simple representation of the axis system to assist the texture descriptions, where SD, RD and CD refer to the shear, rotational and compressive directions, respectively.

The textures were determined near the centres ($r = 0.1$ mm), at the middle or mid-radius positions ($r = 2$ mm) and at the edges ($r = 4$ mm) of the HPT-deformed discs by measuring the incomplete pole figures using a Phillips X-ray texture goniometer. A set of six $\{10\bar{1}0\}$, $\{0002\}$, $\{10\bar{1}1\}$, $\{10\bar{1}2\}$, $\{11\bar{2}0\}$ and $\{10\bar{1}3\}$ measured pole figures was used to calculate the orientation distribution function (ODF) using the MTEX toolbox [31].

The microstructures of the processed samples were investigated using Electron BackScatter Diffraction (EBSD) in the RD-SD plane after mechanical and ionic polishing using a Gatan PECS II system at a high voltage of 5 kV for 15 minutes. The observations were carried out using a scanning electron microscope FEG-SEM SUPRA 55 VP operating at 20 kV. The EBSD step size was 0.1 μm and the EBSD data acquisition and analysis were undertaken using the TSL Orientation Imaging Microscopy, OIM^{TM} software. The grain size data were obtained using a grain tolerance angle of 5° and the minimum grain size was chosen as 5 pixels. All datum points with a confidence index (CI) lower than 0.05 were excluded from the analysis, where the CI quantifies the reliability of the indexed pattern.

4

The Vickers microhardness was measured at the same centre, mid-point and edge positions of the HPT-deformed discs using a SHIMADZU type HMV-2 tester. At least three indentations were used to obtain an average hardness value using a load of 100 g ($Hv_{0.1}$) and a dwell time of 10 s. The dislocation density, ρ, was estimated by analyzing the X-ray diffractometry (XRD) patterns using the Halder–Wagner method [32, 33], where the dislocation density is expressed as [34]:

$$\rho = 2\sqrt{3}\frac{\langle\varepsilon^2\rangle^{1/2}}{Db} \tag{1}$$

where D is the crystallite size, $\langle\varepsilon^2\rangle^{1/2}$ is the microstrain and b is the Burgers vector.

3. Experimental results

3.1 Texture evolution after HPT processing

Figure 3 illustrates the evolution of the texture in terms of the basal (0002) recalculated pole figures measured at the centres, middles and edges of the HPT-deformed discs of the Mg-0.41Dy alloy, respectively. It is noted that the texture of the as-cast alloy is random. Nevertheless, a basal fiber is well developed starting from 1 turn of HPT, although there are some variations in the textures from the centres to the edges of the deformed discs. Firstly, the texture intensity in the centre of the disc is weak and does not change with increasing numbers of HPT turns, whereas the texture intensity in the middle and edge shows a continuous increase upon increasing numbers of turns. Secondly, the textures in the centres of the deformed discs show a typical basal texture where the basal (0002) planes of most grains are oriented parallel to the RD-SD plane. In addition, an asymmetric split of the basal planes, shifted by about 15° in the compression direction towards the shear direction, is visible in the middle and edge of the deformed discs. A similar texture evolution was reported recently in Mg-Nd and Mg-Ce alloys processed by HPT for up 10 turns [35].

5

The texture index I is a useful parameter that quantifies the texture trends and helps in their interpretation. The index may be calculated from the following equation [36]:

$$I = \frac{1}{8\pi^2} \int_G f^2(g) dg \tag{2}$$

where $f(g)$ represents the Orientation Distribution Function (ODF) values and G is the Euler space.

The evolution of the texture index of the Mg-0.41Dy alloy processed by HPT is represented in Figure 4 against the equivalent strain, ε_{eq}, calculated using the equation [37]:

$$\varepsilon_{eq} = \frac{2\pi N r}{h\sqrt{3}} \tag{3}$$

where N, r and h are the numbers of HPT turns, the radial distance from the centre of the disc and the thickness of the disc, respectively.

The texture index increases with increasing numbers of HPT turns in the three selected positions of the HPT-deformed discs where the evolution is consistent with the assumption that the texture sharpens with increasing strain. However, it is also apparent that the texture index in the centre of the HPT-deformed discs is much lower than at the middle and edge positions. Specifically, the texture index slowly increases from 2.12 after 1/4 turn to 3.03 after 5 turns and thereafter appears to saturate. By contrast, there is a rapid increase at the middle and edge positions where I = 2.17 (2.52) after 1/4 turn to I = 3.31 (3.60) after 1 turn at the middle and edge, respectively. Furthermore, the texture index continuously strengthens to reach values of about ~4.0 and ~4.16 after 10 turns at the middle and edge, respectively, and then stabilizes. It should be noted that these results are consistent with the saturation in hardness which is generally observed after ~10 HPT turns [38].

3.2 Microhardness and dislocation density evolution after HPT processing

Figure 5a shows the evolution of the microhardness in the centre, middle and edge of the HPT-deformed discs with increasing numbers of HPT turns. It is apparent that the results

6

fall into three stages. In the first stage, the microhardness increases from 33.5±1.1 Hv for the as-cast condition to 45.6±0.9, 48.9±0.9 and 50.0±1.3 Hv in the centre, middle and edge of the 1/4 turn disc, respectively. During the second stage, the microhardness in these three positions decreases with increasing HPT turns up to 5 turns, and then finally the microhardness shows saturation and reaches essentially a steady-state after 15 turns of 40±0.8, 38±0.6 and 37±0.8 Hv in the centre, middle and edge of the discs, respectively. Thus, after the first stage, for discs processed with more than 1/4 turn, the microhardness values in the centre are higher than those in the middle and edge of the HPT-processed discs.

In Figure 5b, the microhardness values are re-plotted against the equivalent strain, ε_{eq}, and these results demonstrate that the microhardness behavior shows a bell-shaped curve wherein the microhardness increases with increasing equivalent strain at $\varepsilon_{eq} = 4$ ($N = 1/4$ turn) and then decreases to saturation around 37±0.8 Hv at equivalent strains higher than ~40 ($N = 5$ turns) and thereafter remains constant with increasing strain. This means that the highest microhardness was reached at $\varepsilon_{eq} = 4$ ($N = 1/4$ turn).

Figure 6 presents the XRD patterns of the as-received Mg-0.44Dy alloy and in the centre, middle and edge of the HPT-deformed discs. All peaks present in the as-cast alloy belong to the Mg matrix and no additional peaks were observed after HPT processing. As can be seen from Figure 6, HPT processing leads to a slight shift of the matrix (Mg) peaks from their 2θ angular positions for the peaks indicating a distortion of the lattice parameter.

The evolution of dislocation density estimated from the XRD measurements near to the centre, middle and edge of the HPT discs is presented in Figure 7 as a function of the numbers of HPT turns and the equivalent strain, respectively. The dislocation density increases rapidly at low equivalent strains to reach a maximum value of ~4.2×10^{14} m^{-2} at $\varepsilon_{eq} = 6$ ($N = 5$ turns) and decreases to saturate around 3.5×10^{14} m^{-2} at the highest equivalent

7

strains. These results demonstrate, therefore, that the dislocation density near the centres of the discs is higher than at the middle or edge.

3.3 Microstructure evolution after HPT processing

Figure 8 illustrates the Orientation Imaging Micrographs in inverse pole figure (IPF) maps depicting the microstructure of the Mg-0.41Dy alloy after HPT processing near to the three zones of interest after 1/2, 5 and 15 turns. The mean grains size achieved under these conditions is inserted in the top left corner of the images. The extensive black zones in the 1/2 turn discs correspond to the zones with CI values lower than 0.05 and may be attributed to the highly deformed or distorted nature of the samples. A smaller measurement area in the centre of the ½ HPT sample with smaller step size (50 nm) is shown in Figure 9 in order to have a more statistically valid result. It is apparent from Figure 9 that even the individual grains are now better illustrated but nevertheless there remain numerous zones with low CI values and low numbers of grains.

It is also readily apparent that the HPT processing leads to strong grain refinement with a grain size of 0.7±0.1 μm after 15 turns. Similar grain refinements were reported for ZK60 (Mg-5.5Zn-0.5Zr, wt. %) [39] and AZ31 [14] alloys processed at room temperature for up to 5 turns. The grain refinement estimated by transmission electron microscopy was in the range of ~200–300 nm after HPT processing of an AZ80 alloy [40] and an Mg-22Gd (wt. %) alloy [26], respectively. It appears also that the grain size decreases with increasing numbers of HPT turns and with increasing radial distance, although there is a clear saturation after about 5 turns.

The grain boundary misorientation angle distributions of the Mg-0.41Dy alloy after HPT processing near to the centre, middle and edge after 5 and 15 turns are also shown in Figure 8. It is to be noted that the grain boundary misorientation angle distributions after ½ turn are not

presented because of a lack of reasonable statistics. The microstructures after 5 and 15 HPT

turns exhibit a significant fraction of boundaries with misorientations around 30° which

correspond to the basal texture [41].

4. Discussion

It is well established and evident from equation (3) that the strain distribution in the

HPT discs is inhomogeneous and depends on the radial distance from the centre of the disc.

This means it is reasonable to anticipate an inhomogeneities in the texture, microstructure and

microhardness of discs processed by HPT [42]. It should be noted also that during HPT

processing the discs undergo additional plastic deformation caused by the high imposed

compressive pressure [43].

The development of a basal texture during the early stages of deformation, as shown in

Figure 3, is attributed to the activation of twinning and mostly by extension twinning

$\{10\bar{1}2\}<10\bar{1}\bar{1}>$. In this case, the c-axis of the crystals is re-oriented by 86.8° so that it is

nearly parallel to the loading or compression direction [14]. As a consequence with

subsequent strain increase, the basal slip <a> $\{0001\}<11\bar{2}0>$ will accommodate the shear and

hence grains with a basal plane will maintain their orientation [14]. The tilted texture of 15°

towards the SD observed in the middle and edge of the HPT samples is due to the activation

of other deformation modes such as prismatic slip on <a>$\{10\bar{1}0\}<\bar{1}2\bar{1}0>$ and/or pyramidal

slip on <c+a> $\{11\bar{2}2\}<11\bar{2}3>$ [44]. The weaker basal texture developed in the present alloy,

or in Mg-RE (RE = Nd, Ce alloys [35]) in general relative to the AZ31 Mg alloy [14], is

explained by the effect of RE elements in promoting the <a> prismatic and <c+a> pyramidal

slip systems. This effect is attributed to the decrease in stacking fault energy and the reduction

in dislocation motion and the ability to cross slip as the solutes diffuse in the dislocation cores

[1]. It is apparent from Figure 8 that no twins were detected in the microstructures after 5 and

15 HPT turns. Indeed, the misorientation angle distribution for both samples exhibit very low fractions around 56 and 86° which correspond to rotation orientation relationships between the $\{10\bar{1}1\}$ compression twin, $\{10\bar{1}2\}$ extension twin and the matrix [45], respectively. On the contrary, it was reported that the fraction of activated twins increases along the radial direction of the Mg-Gd-Y-Zr alloy processed by HPT through 5 turns [15]. In addition, a high fraction of tensile twinning (86.18°/$<2\bar{1}\bar{1}0>$) was reported in an as-cast Mg-Dy-Al-Zn-Zr alloy processed by HPT for up 3 turns [46]. Nevertheless, it is well known that an inhibition in mechanical twinning depends strongly on the influence of solute elements [47], secondary particles [48] and the grain size [49] in the deformed alloy.

In the present study, and in agreement with the assumption of Rokhlin [50], no secondary particles are expected in the Mg-0.41Dy alloy since the solubility value of Dy is high in the solid Mg matrix: specifically, 24.5 wt.% at 540 °C and 10.2wt.% at 200 °C. It has been demonstrated that the RE addition of the Yttirium sub-group, such as Dy, may effectively suppress the activation of twinning in the $\{10\bar{1}2\}$ directions [47]. Finally and as recently reported, there is a critical grain size of ~2.7 μm in Mg-based alloys such that twinning dominates above this value and at smaller grain sizes there is only dislocation slip [49]. As shown in Figure 8, the grain size after HPT processing was in range of ~0.75 – 1.2 μm and therefore the activation of twining is not expected. Certainly the occurrence of mechanical twinning in the Mg-Gd-Y-Zr and Mg-Dy-Al-Zn-Zr alloys after HPT processing [15, 46] may be associated with the absence of any considerable grain refinement. Moreover, it has been shown that twinning is a primary factor that accommodates plastic deformation under conditions of coarse grains at relatively low strain levels such as after 1/4 turn [27]. Thus, increasing the numbers of HPT turns eliminates the twin boundaries caused by twin interactions with other twins or with grain boundaries and dislocations [27]. At this stage, the

available high strain energy can activate the prismatic and pyramidal slip systems in order to ensure more independent slip systems and maintain compatibility [27].

The microhardness evolution shown in Figure 5 is consistent with one of the three models reported for hardness evolution in UFG materials processed by HPT: (1) strain hardening without recovery, (2) strain hardening with recovery and (3) strain softening [51, 52]. Specifically, the occurrence of hardening and then softening denotes a rapid recovery. In the present investigation the microhardness initially increases with strain because of the high dislocation density introduced in the material, it reaches a maximum at $N = 1/4$ turn and thereafter it decreases to a saturation condition which commences at $N = 5$ turns due to a recovery mechanism.

It is interesting to evaluate the degree of strain hardening or softening behavior occurring during HPT using the microhardness measurements, Hv, from the following equation [39]:

$$Hv = K\varepsilon_{eq}^n \tag{4}$$

where K and n are a material constant and the hardenability exponent, respectively. This latter exponent corresponds to the slope in a double logarithmic plot of the microhardness values as a function of the equivalent strain.

Figure 10 shows the evolution of logarithmic Hv against logarithmic ε_{eq} where the values of Hv were taken from Figure 5. It is readily apparent that in the first stage the exponent n is positive (0.03) revealing a strain hardening whereas in the second stage there is a negative hardening exponent (-0.03) associated with a strain softening. The present Mg-0.41Dy alloy processed by HPT demonstrated a weak strain hardening behavior compared to the AZ31 and ZK60 alloys with n values of 0.08 [52] and 0.07 [39, 53], respectively. However, it was also reported that the strain hardening rate is dependent on the initial state

prior to the HPT processing [23]. Therefore, the *n* exponent was reported lower (~0.05) for an as-cast alloy processed by HPT than for a solutioned alloy processed by HPT (~0.09) [23].

Figures 5 and 7 provide evidence that with more than 1/4 turn the microhardness and dislocation density values in the centre are higher than those in the middle and edge of the HPT-deformed discs. A similar microhardness evolution was reported for pure Mg processed by HPT at room temperature [17, 54]. However, this type of evolution is not consistent with equation (3) where the microhardness is expected to increase with increasing radial distance from the centre of the disc [14, 22, 40, 43, 46, 53].

A reasonable explanation for this inverse behavior is that the edge area accumulates a higher strain than the centre so that the critical strain for dynamic recrystallization is attained more easily in the edge and middle areas, thereby causing a softening in these regions. This is consistent with the general explanation for this type of inverse behavior that it requires an exceptionally high rate of dynamic recovery [55]. Thus, pure Mg samples processed by HPT at room temperature exhibited a decrease in microhardness with increasing distance from the centre after 1, 3 and 10 turns [17]. Furthermore, TEM analysis demonstrated that hardening in the centre was due to the high dislocation density whereas softening in the edge areas was attributed to recrystallization mechanisms [17]. In practice, the occurrence of recovery or recrystallization at large strains is associated with the relatively low melting temperature of Mg (650 °C) [17] such that in the saturation stage starting from 5 turns the deformation energy is transformed to heat rather than additional defects and this leads to dynamic recovery or recrystallization [56].

It is possible to identify the recrystallized grain fraction from EBSD data using the Grain Orientation Spread (GOS) approach implemented in the OIM^{TM} software. The recrystallized grains may be distinguished from the deformed grains on the basis of a maximum GOS value of 1° [57]. Figures 11 and 12 give an estimation of the fraction of

recrystallized grains during HPT processing through 5 and 15 turns. As can be seen, both samples exhibit a recrystallized microstructure and the fraction of grains with a GOS value $\leq$ 1° increases from the centre ($\sim$ 46 %) towards the edge ($\sim$ 58.6 %) after 5 turns. In addition, the microstructure after 15 turns contains about 77 % of recrystallized grains and appears to be reasonably homogeneous along the radius from the centre to the edge of the HPT disc.

A close analysis of Figure 11 shows that the steady-state after 15 turns appears to exhibit a bimodal microstructure in the centre, middle and edge of the sample. Thus, the distribution of grains size in the centre, middle and edge of the 15 HPT sample presented in Figure 13 show that 53% of the grains have sizes below 0.7 μm and 47% of grains are larger than 1μm in the centre after 15 turns. In the middle of the disc, 77% of grains are less than 1 μm and 23% of grains have more than 1.2 μm. Finally, the fraction of grains at the edge having sizes less than 1 μm is 48% whereas 52% are larger than 1.2 μm. A similar bimodal microstructure with larger recrystallized grains ($\sim$1 μm) was reported in the steady-state condition for pure Mg processed by HPT [17]. In practice, the grain refinement mechanism in hexagonal close-packed (HCP) metals results from a dynamic recrystallization process [58, 59] wherein new finer grains are formed along the grain boundaries of the initial coarse structure leading to the development of a bimodal grain structure. These finer grains then gradually occupy the larger coarser grains with increasing straining and thereby produce an ultrafine microstructure [17, 18].

4. *Hardening mechanisms during HPT processing*

The strengthening, represented by σ_y, of metals and alloys induced by HPT processing at room temperature is generally attributed to the concomitant occurrence of dislocation hardening, $\Delta\tau_d$, and grain size hardening, $\Delta\sigma_G$, so that [60]:

$$\sigma_y = \Delta\tau_d + \Delta\sigma_G \tag{6}$$

The increment of the critical resolved shear stress due to dislocations, $\Delta\tau_d$, is given by [60]:

$$\Delta\tau_d = \alpha_1 M G b \sqrt{\rho} \tag{7}$$

where α_1, M and G are a constant of ~0.3, the Taylor factor and the shear modulus (17.7 GPa for Mg [22]).

The effect of grain refinement is usually evaluated by the Hall-Petch equation [60]:

$$\Delta\sigma_G = \frac{k_{HP}}{\sqrt{d}} \tag{8}$$

where k_{HP} is the Hall–Petch constant (~40.7 MPa/ $\mu m^{-1/2}$ for Mg [22]), and d is the mean grain size.

The relationship between hardness, Hv, and the yield strength, σ_y, can be approximated by the relationship [61]:

$$Hv = C\,\sigma_y \tag{9}$$

where C is a constant having a value of ~0.3.

The compilation of different values of grain size hardening and dislocation hardening estimated in the centre, middle and edge of the 1/2, 5 and 15 turn discs are presented in Table 1. As shown, the effect of dislocation hardening is higher than for the grain size. By contrast, the effect of grain size hardening was more pronounced in as-cast and solution-treated Mg-8.2Gd-3.8Y-1.0Zn-0.4Zr (wt. %) alloy processed by HPT at room temperature [22, 23].

It is worth noting that in the 5 and 15 turns discs the difference between the experimental values of microhardness and those measured from the grain size and dislocations is in the range of ~ 4 – 5 Hv, which is close to the microhardness value of undeformed pure Mg (~ 6 Hv) [60]. Therefore, the hardening mechanism in the 1/2 turn disc does not follow the same trend since the difference between the experimental and calculated values is close to ~13.5 Hv. In practice, texture strengthening is considered to play an important role in the rapid hardening in the early stage of deformation [35, 62]. Thus, as can

14

be seen from Figure 3, the change of grain orientation from random to a basal texture after 1/4 and 1/2 turn, where (0002) is perpendicular to the leading direction of the microhardness tests, leads to an increase in the microhardness values.

5. Summary and conclusions

1. An Mg-0.41Dy alloy was severely deformed by high-pressure torsion at room temperature for up to 15 turns and it is shown that a basal (0002) fiber texture is developed starting from 1 HPT turn with some differences between the centre to edge of the HPT-deformed discs.

2. The texture intensity in the centre of the disc was weak and was not changed with increasing numbers of HPT turns, whereas there was a continuous increase upon increasing the numbers of turns in the middle and edge regions of the deformed discs. The texture index slowly increased from 2.12 after 1/4 turn to 3.03 after 5 turns and appeared to saturate thereafter.

3. The microhardness increasesd with a positive strain hardenability of ~0.03 from 33.5 *Hv* for the as-cast state to ~50 *Hv* and then decreased with a negative strain hardenability of about -0.03 with increasing HPT processing up to 5 turns and finally reached a steady-state at 15 turns of about 40 *Hv*.

4. A significant grain refinement to ~0.75 μm was evident after room temperature HPT processing. The steady-state after 15 turns exhibited a relatively bimodal microstructure with a major part of the grains having a size of less than ~0.7 μm and the other part exceeding ~1 μm. No traces of twins were detected in these microstructures.

5. The microstructure after 15 HPT turns contained about 77 % of recrystallized grains and appeared to be homogeneous along the radial distance from the centre of the HPT disc.

6. In addition to dislocation and grain hardening, it is concluded that texture strengthening makes a significant contribution to the rapid increase in hardening in the early stages of deformation.

Acknowledgements

References

[1] A. Imandoust, C.D. Barrett, T. Al-Samman, K.A. Inal, H. El Kadiri, A review on the effect of rare-earth elements on texture evolution during processing of magnesium alloys, J. Mater. Sci. 52 (2017) 1–29.

[2] S. You, Y. Huang, K.U. Kainer, N. Hort, Recent research and developments on wrought magnesium alloys, J. Magnesium and Alloys 5 (2017) 239–253.

[3] L.W.F. Mackenzie, F.J. Humphreys, G.W. Lorimer, K. Savage, T. Wilks, in: K.U. Kainer (Ed.) Magnesium Alloys and their Applications, DGM, Germany (2003) 158.

[4] T. Al-Samman. Modification of texture and microstructure of magnesium alloy extrusions by particle stimulated recrystallization, Mater. Sci. Eng. A 560 (2013) 561–566.

[5] H. Yan, S. Xu, R. Chen, S. Kamado, T. Honma, E. Han, Twins, shear bands and recrystallization of a Mg–2.0% Zn–0.8% Gd alloy during rolling, Scripta Mater. 64 (2011) 141–144.

[6] S. Sandlöbes, S. Zaefferer, I. Schestakow, S. Yi, R. Gonzalez-Martinez, On the role of non-basal deformation mechanisms for the ductility of Mg and Mg–Y alloys, Acta Mater. 59 (2011) 429–439.

[7] J. Bohlen, S. Yi, D. Letzig, K.U. Kainer, Effect of rare earth elements on the microstructure and texture development in magnesium–manganese alloys during extrusion, Mater. Sci. Eng. A 527 (2010) 7092–7098.

[8] C.D. Barrett, H. El Kadiri, The roles of grain boundary dislocations and disclinations in the nucleation of $\{10\bar{1}2\}$ twinning, Acta Mater. 63 (2014) 1–15.

[9] N. Stanford. Micro-alloying Mg with Y, Ce, Gd and La for texture modification—A comparative study, Mater. Sci. Eng. A 527 (2010) 2669–2677.

[10] N. Stanford, M.R. Barnett, The origin of "rare earth" texture development in extruded Mg-based alloys and its effect on tensile ductility, Mater. Sci. Eng. A 496 (2008) 399–408.

[11] N. Stanford, D. Atwell, A. Beer, C. Davies, M.R. Barnett, Effect of microalloying with rare-earth elements on the texture of extruded magnesium-based alloys, Scripta Mater. 59 (2008) 772–775.

[12] Z.J. Yu, Y.D. Huang, X. Qiu, G.F. Wang, F.Z. Meng, N. Hort, J. Meng, Fabrication of a high strength Mg–11Gd–4.5Y–1Nd–1.5Zn–0.5Zr (wt%) alloy by thermomechanical treatments, Mater. Sci. Eng. A 622 (2015) 121–130.

[13] J.L. Wang, H.W. Dong, L.D. Wang, Y.M. Wu, L.M. Wang. Effect of hot rolling on the microstructure and mechanical properties of Mg–5Al–0.3Mn–2Nd alloy, J. Alloys Compds 507 (2010) 178–183.

[14] Y. Huang, R.B. Figueiredo, T. Baudin, A-L.Helbert, F. Brisset, T.G. Langdon, Microstructure and texture evolution in a magnesium alloy during processing by high-pressure torsion, Mater. Res. 16 (2013) 577–585.

[15] L. Tang, Y. Zhao, N. Liang, R.K. Islamgaliev, R.Z. Valiev, Y.T. Zhu, Localized deformation via multiple twinning in a Mg–Gd–Y–Zr alloy processed by high-pressure torsion, Mater. Sci. Eng. A 677 (2016) 68–75.

[16] Y. Huang, R.B. Figueiredo, T.G. Langdon. Effect of HPT processing temperature on strength of a Mg–Al–Zn alloy, Rev. Adv. Mater. Sci. 31 (2012) 129–137.

[17] K. Edalati, A. Yamamoto, Z. Horita, T. Ishihara, High-pressure torsion of pure magnesium: Evolution of mechanical properties, microstructures and hydrogen storage capacity with equivalent strain, Scripta Mater. 64 (2011) 880–883.

[18] R.B. Figueiredo, S. Sabbaghianrad, A. Giwa, J.R. Greer, T.G. Langdon, Evidence for exceptional low temperature ductility in polycrystalline magnesium processed by severe plastic deformation, Acta Mater. 122 (2017) 322–331.

[19] C.L.P. Silva, I. C. Tristão, S. Sabbaghianrad, S.A. Torbati-Sarraf, R.B. Figueiredo, T.G. Langdon. Microstructure and hardness evolution in magnesium processed by HPT, Mater. Res. 20(Suppl.1) (2017) 2–7.

[20] A.S.J. Al-Zubaydi, A.P. Zhilyaev, S.C. Wang, P. Kucita, P.A.S. Reed, Evolution of microstructure in AZ91 alloy processed by high-pressure torsion, J. Mater. Sci. 51 (2016) 3380–3389.

[21] C.L.P. Silva, A.C. Oliveira, C.G.F. Costa, R.B. Figueiredo, M.deF. Leite, M.M. Pereira, V.F.C. Lins, T.G. Langdon, Effect of severe plastic deformation on the biocompatibility and corrosion rate of pure magnesium, J. Mater. Sci. 52 (2017) 5992–6003.

[22] W.T. Sun, C. Xu, X.G. Qiao, M.Y. Zheng, S. Kamado, N. Gao, M.J. Starink, Evolution of microstructure and mechanical properties of an as-cast Mg- 8.2Gd-3.8Y-1.0Zn-0.4Zr alloy processed by high pressure torsion, Mater. Sci. Eng. A 700 (2017) 312–320.

[23] W.T. Sun, X.G. Qiao, M.Y. Zheng, C. Xu, N. Gao, M.J. Starink, Microstructure and mechanical properties of a nanostructured Mg-8.2Gd-3.8Y-1.0Zn-0.4Zr supersaturated solid solution prepared by high pressure torsion, Mater. Des. 135 (2017) 366–376.

[24] R. Alizadeh, R. Mahmudi, A.H.W. Ngan, Y. Huang, T.G. Langdon, Superplasticity of a nano-grained Mg-Gd-Y-Zr alloy processed by high-pressure torsion, Mater. Sci. Eng. A 651 (2016) 786–794.

[25] S.V. Dobatkin, L.L. Rokhlin, E.A. Lukyanova, M.Y. Murashkin, T.V. Dobatkina, N.Y. Tabachkova, Structure and mechanical properties of the Mg-Y-Gd-Zr alloy after high pressure torsion, Mater. Sci. Eng. A 667 (2016) 217–223.

[26] J. Čížek, P. Hruška, T. Vlasák, M. Vlček, M. Janeček, P. Minárik, T. Krajňák, M. Šlapáková, M. Dopita, R. Kužel, T. Kmječ, J.G. Kim, H.-S. Kim, Microstructure development of ultra fine grained Mg-22 wt%Gd alloy prepared by high pressure torsion, Mater. Sci. Eng. A 704 (2017) 181–191.

[27] J. Bai, F. Xue, S.N. Alhajeri, T.G. Langdon, Microstructural evolution of Mg-4Nd alloy processed by high-pressure torsion, Mater. Sci. Forum 667-669 (2011) 391–396.

[28] O.B. Kulyasova, R.K. Islamgaliev, A.R. Kil'mametov, R.Z. Valiev, Superplastic behavior of magnesium-based Mg–10 wt % Gd Alloy after severe plastic deformation by torsion, Phys. Metals Metallog. 101 (2006) 585–590.

[29] R.B. Figueiredo, P.R. Cetlin, T.G. Langdon, Using finite element modeling to examine the flow processes in quasi-constrained high-pressure torsion, Mater. Sci. Eng. A 528 (2011) 8198–8204.

[30] R.B. Figueiredo, P.H.R. Pereira, M.T.P. Aguilar, P.R. Cetlin, T.G. Langdon, Using finite element modeling to examine the temperature distribution in quasi-constrained high-pressure torsion, Acta Mater. 60 (2012) 3190–3198.

[31] R. Hielscher, H. Schaeben, A novel pole figure inversion method: specification of the MTEX algorithm, J. Appl. Cryst. 41 (2008) 1024–1037.

[32] N.C. Halder, C.N.J. Wagner, Separation of particle size and lattice strain in integral breadth mesurements, Acta Cryst. 20 (1966) 312–313.

[33] J.I. Langford, A rapid method for analysing the breadths of diffraction and spectral lines using the Voigt function, J. Appl. Cryst. 11 (1978) 10–14.

[34] R.Z. Valiev, R.K. Islamgaliev, I.V. Alexandrov, Bulk nanostructured materials from severe plastic deformation, Prog. Mater. Sci. 45 (2000) 103–189.

[35] Y.I. Bourezg, H. Azzeddine, Y. Huang, D. Bradai, T.G. Langdon, Texture and microhardness of Mg-Rare Earth (Nd and Ce) alloys processed by high-pressure torsion, Mater. Sci. Eng. A 724 (2018) 477–485.

[36] U.F. Kocks, C.N. Tomé, H.R. Wenk, Texture and Anisotropy: Preferred Orientations in Polycrystals and Their Effect on Materials Properties, Cambridge University Press, 2000.

[37] F. Wetscher, A. Vorhauer, R. Stock, R. Pippan, Structural refinement of low alloyed steels during severe plastic deformation, Materials Science and Engineering A 387–389 (2004) 809–816.

[38] S. Sabbaghianrad, T.G. Langdon, An evaluation of the saturation hardness in an ultrafine-grained aluminum 7075 alloy processed using different techniques, J. Mater. Sci. 50 (2015) 4357–4365.

[39] S.A. Torbati-Sarraf, S. Sabbaghianrad, R.B. Figueiredo, T.G. Langdon, Orientation imaging microscopy and microhardness in a ZK60 magnesium alloy processed by high-pressure torsion, J. Alloys Compds 712 (2017) 185–193.

[40] S.A. Alsubaie, P. Bazarnik, M. Lewandowska, Y. Huang, T.G. Langdon, Evolution of microstructure and hardness in an AZ80 magnesium alloy processed by high-pressure torsion, J. Mater. Res. Technol. 5 (2016) 152–158.

[41] J.A. del Valle, M.T. Perez-Prado, O.A. Ruano, The distribution of disorientation angles in a rolled AZ31 Mg alloy, Rev. Metal. Madr. 38 (2002) 353–357.

[42] M. Kawasaki, H-J. Lee, B. Ahn, A.P. Zhilyaev, T.G. Langdon, Evolution of hardness in ultrafine-grained metals processed by high-pressure torsion, J. Mater. Res. Technol. 3 (2014) 311–318.

[43] H.J. Lee, B. Ahn, M. Kawasaki, T.G. Langdon, Evolution in hardness and microstructure of ZK60A magnesium alloy processed by high-pressure torsion, J. Mater. Res. Technol. 4 (2015) 18–25.

[44] S. Agnew, M. Yoo, C. Tome, Application of texture simulation to understanding mechanical behavior of Mg and solid solution alloys containing Li or Y, Acta Mater. 49 (2001) 4277–4289.

[45] P.G. Partridge, The crystallography and deformation modes of hexagonal close-packed metals, Metall. Rev. 12 (1967) 169–194.

[46] R. Kocich, L. Kuncicka, P. Kral, T. C. Lowe, Texture, deformation twinning and hardening in a newly developed Mg–Dy–Al–Zn–Zr alloy processed with high pressure torsion, Mater. Des. 90 (2016) 1092–1099.

[47] K.H. Eckelmeyer, R.W. Herzberg, Deformation in wrought Mg 9 wt.% Y, Metall, Mater. Trans. 1 (1970) 3411–3414.

[48] N. Stanford, M. Barnett, Effect of composition on the texture and deformation behaviour of wrought Mg alloys, Scripta Mater. 58 (2008) 179–182.

[49] H. Fan, S. Aubry, A. Arsenlis, J.A. El-Awady, Grain size effects on dislocation and twinning mediated plasticity in magnesium, Scripta Mater. 112 (2016) 50–53.

[50] L.L. Rokhlin, Magnesium Alloys Containing Rare Earth Metals, Taylor & Francis, New York (2003).

[51] M. Kawasaki, Different models of hardness evolution in ultrafine-grained materials processed by high-pressure torsion, J. Mater. Sci. 49 (2014) 18–34.

[52] M. Kawasaki, R.B. Figueiredo, Y. Huang, T.G. Langdon, Interpretation of hardness evolution in metals processed by high-pressure torsion, J. Mater. Sci. 49 (2014) 6586–6596.

[53] S.A. Torbati-Sarraf, T.G. Langdon, Mechanical properties of ZK60 magnesium alloy processed by high-pressure torsion, Adv. Mater. Res. 922 (2014) 767–772.

[54] M. Joshi, Y. Fukuta, S. Gao, N. Park, D. Terada, N. Tsuji, Fabrication of fine recrystallized grains and their mechanical property in HPT processed pure magnesium, IOP Conf. Series: Mater. Sci. Eng. 63 (2014) 012074.

[55] C. Xu, Z. Horita, T.G. Langdon, The evolution of homogeneity in processing by high-pressure torsion, Acta Mater. 55 (2007) 203–212.

[56] A.P. Zhilyaev, T.G. Langdon, Using high-pressure torsion for metal processing: fundamentals and application, Prog. Mater. Sci. 53 (2008) 893–979.

[57] J.H. Cho, A. Rollett, K. Oh, Determination of a mean orientation in electron backscatter diffraction measurements, Metall. Mater. Trans. A 36 (2005) 3427–3428.

[58] R.B. Figueiredo, T.G. Langdon, Principles of grain refinement in magnesium alloys processed by equal-channel angular pressing, J. Mater. Sci. 44 (2009) 4758–4762.

[59] R.B. Figueiredo, T.G. Langdon, Grain refinement and mechanical behaviour of a magnesium alloy processed by ECAP, J. Mater. Sci. 45 (2010) 4827–4836.

[60] M.J. Starink, X. Cheng, S. Yang, Hardening of pure metals by high-pressure torsion: a physically based model employing volume-averaged defect evolutions, Acta Mater. 61 (2013) 183–192.

[61] J.A. Brinell, Brinell's method of determining hardness and other properties of iron and steel, J. Iron. Steel Inst. 59 (1901) 243–298.

[62] X.G. Qiao, Y.W. Zhao, W.M. Gan, Y.C. Ming, Y. Zheng, K. Wu, N. Gao, M.J. Starink, Hardening mechanism of commercially pure Mg processed by high pressure torsion at room temperature, Mater. Sci. Eng. A 619 (2014) 95–106.

Figure caption

Figure 1. Microstructure of the as-cast Mg-0.44Dy alloy.

Figure 2. Representation of axis system to assist the texture description. SD, RD and CD correspond to the shear, rotation and compression directions, respectively.

Figure 3. Basal (0002) recalculated pole figures near the centre, middle and the edge of the discs of the Mg-0.41Dy alloy processed by HPT at room temperature to 15 turns.

Figure 4. Evolution of texture index of the Mg-0.41Dy alloy as a function of equivalent strain.

Figure 5. Evolution of Vickers microhardness as a function of: a) numbers of HPT turns and b) equivalent strain for the Mg-0.41Dy alloy processed by HPT for up to 15 turns.

Figure 6. XRD patterns of as received Mg-Dy alloy and in the centre, middle and edge of the HPT-deformed discs.

Figure 7. Evolution of dislocation density as a function of : a) numbers of HPT turns and b) equivalent strain for the Mg-0.41Dy alloy processed by HPT for up to 15 turns.

Figure 8. IPF maps in the RD-SD plane (distribution of crystallographic direction parallel to CD) showing the microstructures of the Mg-0.41Dy alloy after HPT near the centre, middle and edge of each disc after processing through 1/2, 5 and 15 turns. Grain boundary misorientation angle distributions of the Mg-0.41Dy alloy after HPT processing near to the centre, middle and edge after 5 and 15 turns.

Figure 9. IPF map showing the microstructure near the centre of ½ HPT disc measured with smaller step size (50 nm).

Figure 10. Evolution of logarithmic Hv as a function of logarithmic ε_{eq} for the Mg-0.41Dy alloy processed by HPT at room temperature for up to 15 turns.
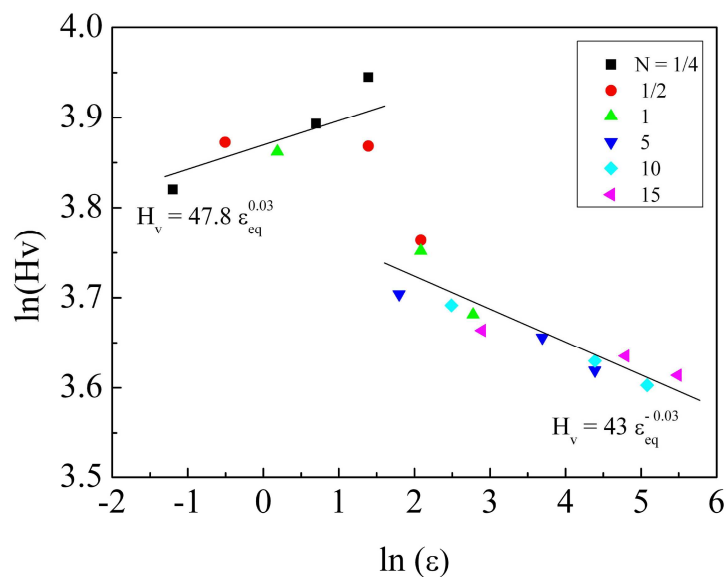
Figure 11. Grain Orientation Spread (GOS) maps of the Mg-0.41Dy alloy after HPT near to the centre, middle and the edge of each disc after processing through 5 and 15 turns.
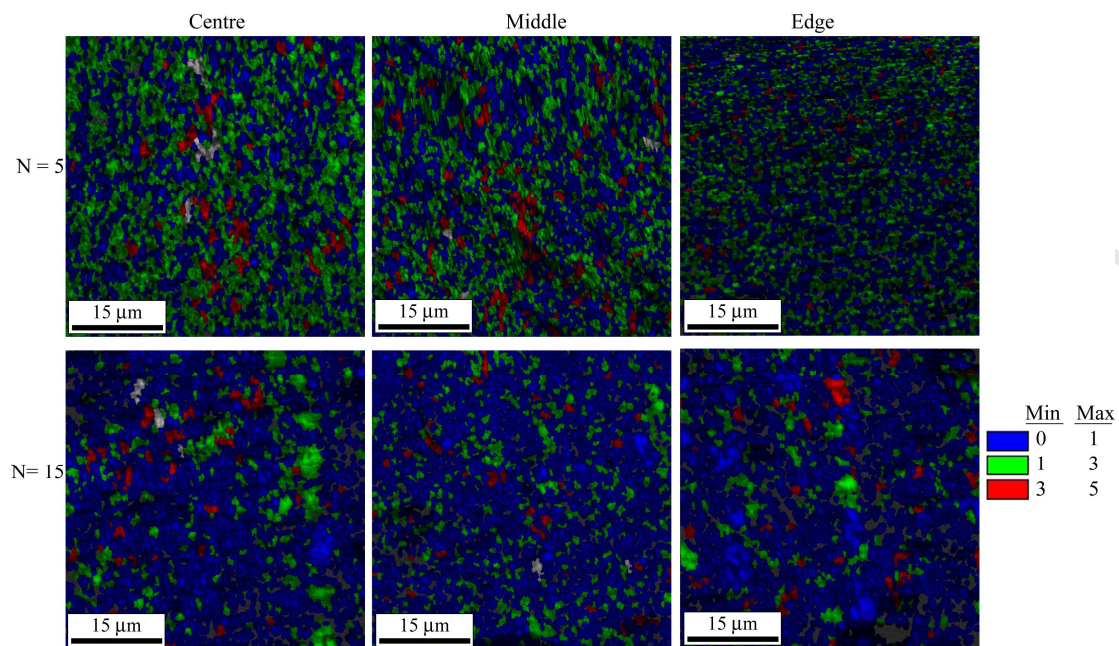
Figure 12. Grain Orientation Spread (GOS) fractions in particular misorientation angle ranges as a function of position inside the discs after processing through 5 and 15 turns.
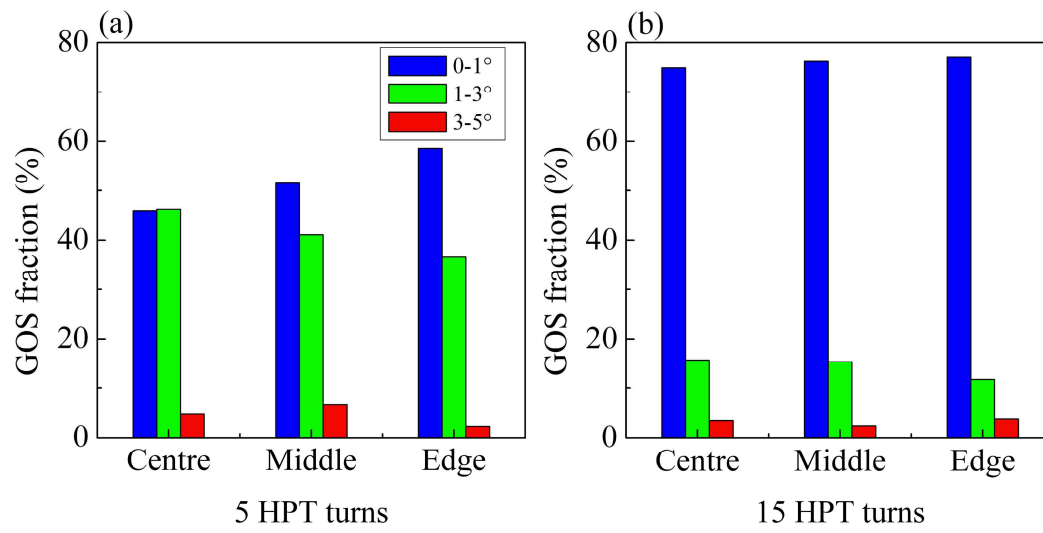
Figure 13. Grain size distribution in the Mg-0.41Dy sample after 5 HPT sample near : a) centre, b) middle and c) edge.
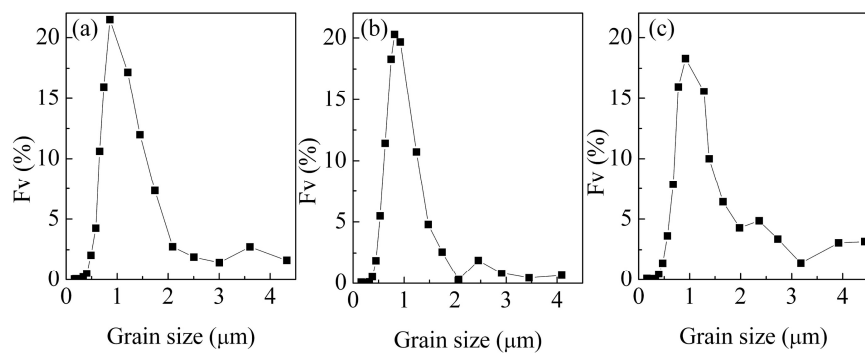
Table 1. Values of experimental microhardness (see Figure 5) and calculated grain size and dislocation hardening for 1/2, 5 and 15 turns.
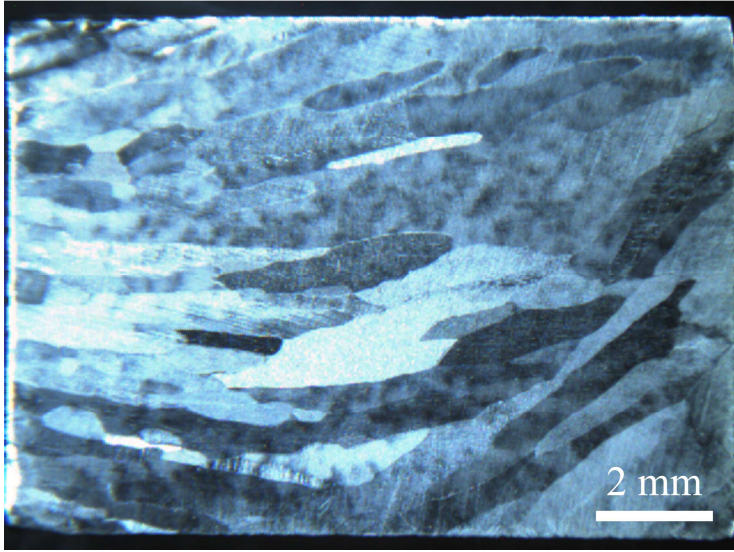
	1/2 turn			5 turns			15 turns		
	Centre	Middle	Edge	Centre	Middle	Edge	Centre	Middle	Edge
Hv	48.3	47.9	43.1	40.6	38.7	37.3	39	37.9	37.1
$C\Delta\,\sigma_G$	11.1	11.7	12.1	12.9	13.9	13.8	13.2	14.1	13.7
$C\Delta\,\tau_d$	18.4	17.7	17.9	21.1	20.2	19.3	20.4	19.8	19.3

	Centre	Middle	Edge
N = 5			
N = 15			

Min	Max
0	1
1	3
3	5

Centre   Middle   Edge

CD

(0002)

N = 1/4

SD   RD

max: 6.6 mrd   max: 6.1 mrd   max: 7.4 mrd

N = 1/2

max: 7.7 mrd   max: 6.7 mrd   max: 9 mrd

N = 1

max: 4.7 mrd   max: 8.8 mrd   max: 9.4 mrd

N = 5

max: 7.9 mrd   max: 9.8 mrd   max: 11 mrd

N = 10

max: 7 mrd   max: 10 mrd   max: 11 mrd

N = 15

max: 6.8 mrd   max: 9.2 mrd   max: 11 mrd

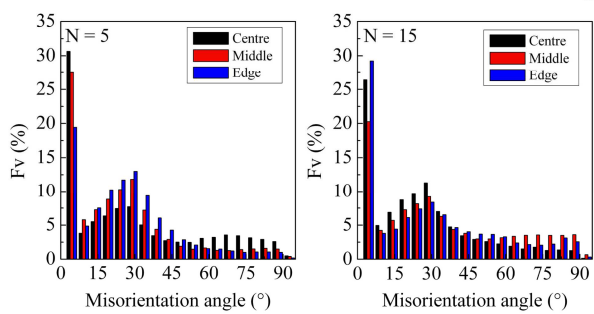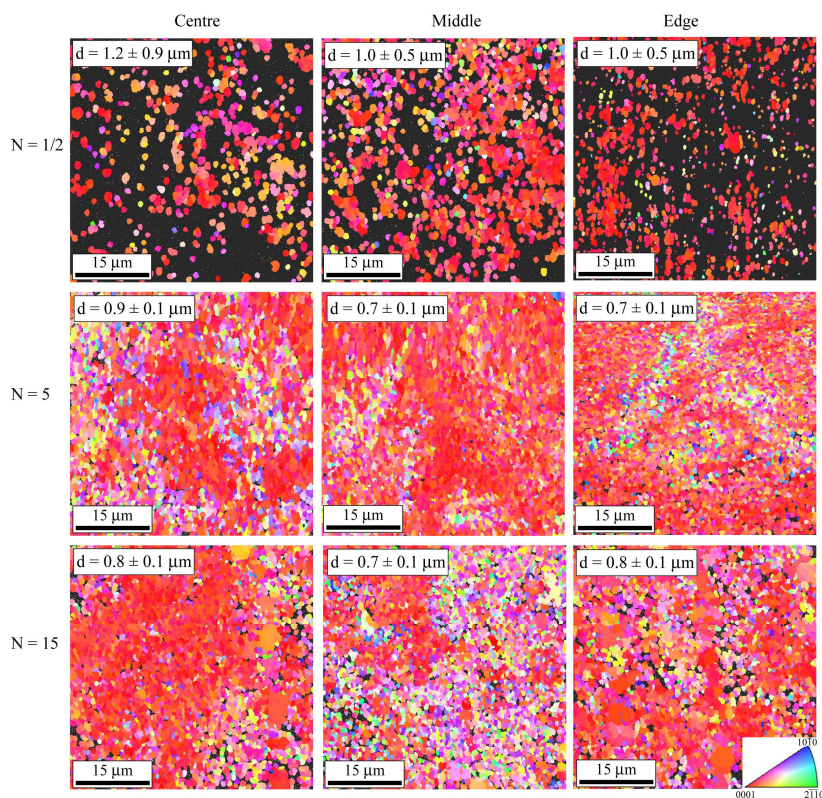|	Centre	Middle	Edge
N = 1/2	d = 1.2 ± 0.9 μm	d = 1.0 ± 0.5 μm	d = 1.0 ± 0.5 μm
N = 5	d = 0.9 ± 0.1 μm	d = 0.7 ± 0.1 μm	d = 0.7 ± 0.1 μm
N = 15	d = 0.8 ± 0.1 μm	d = 0.7 ± 0.1 μm	d = 0.8 ± 0.1 μm
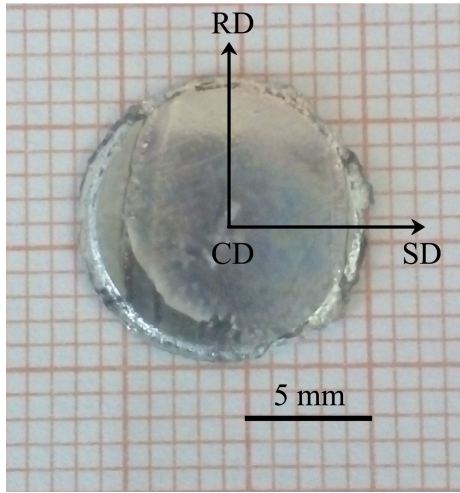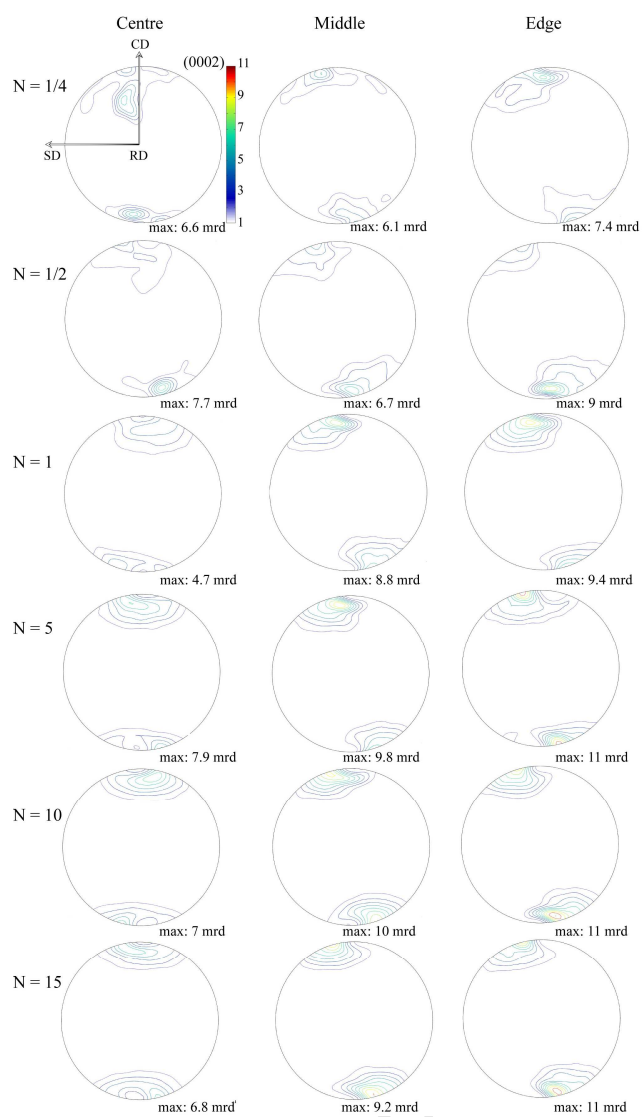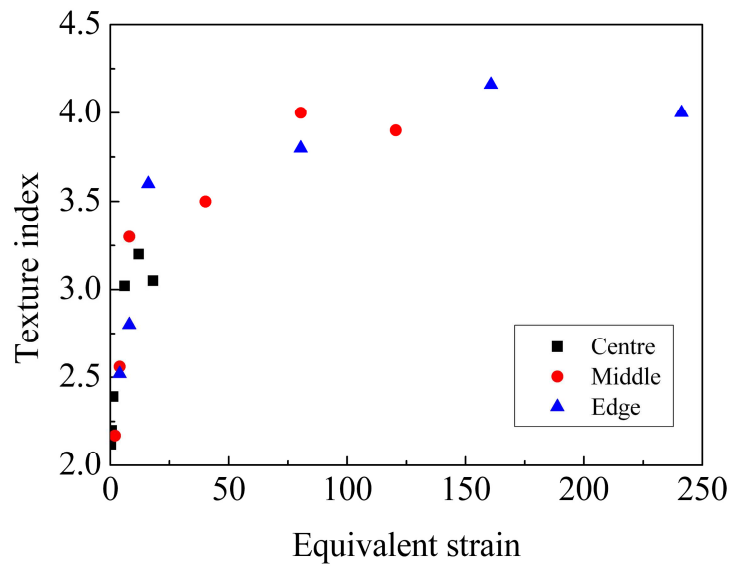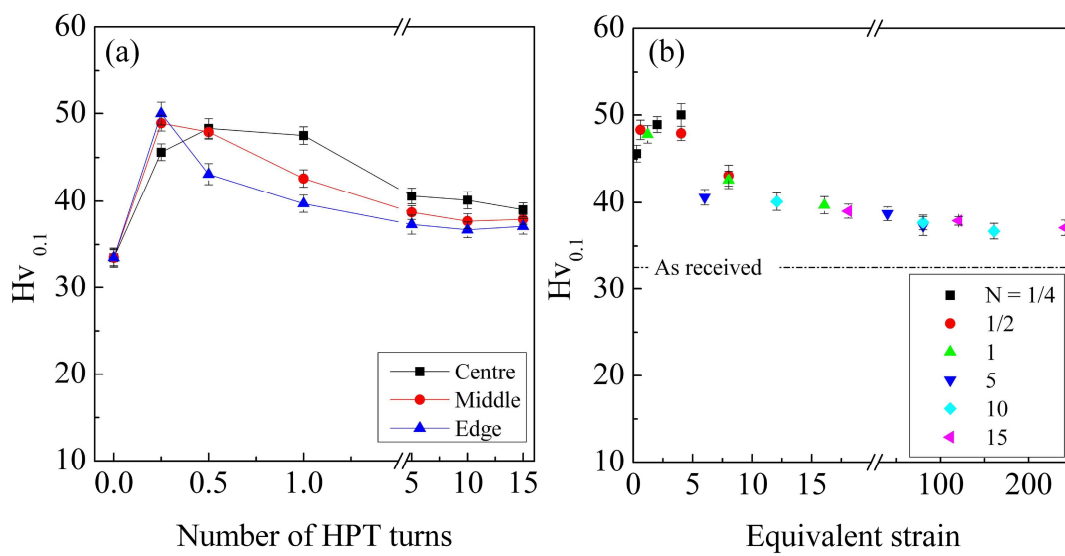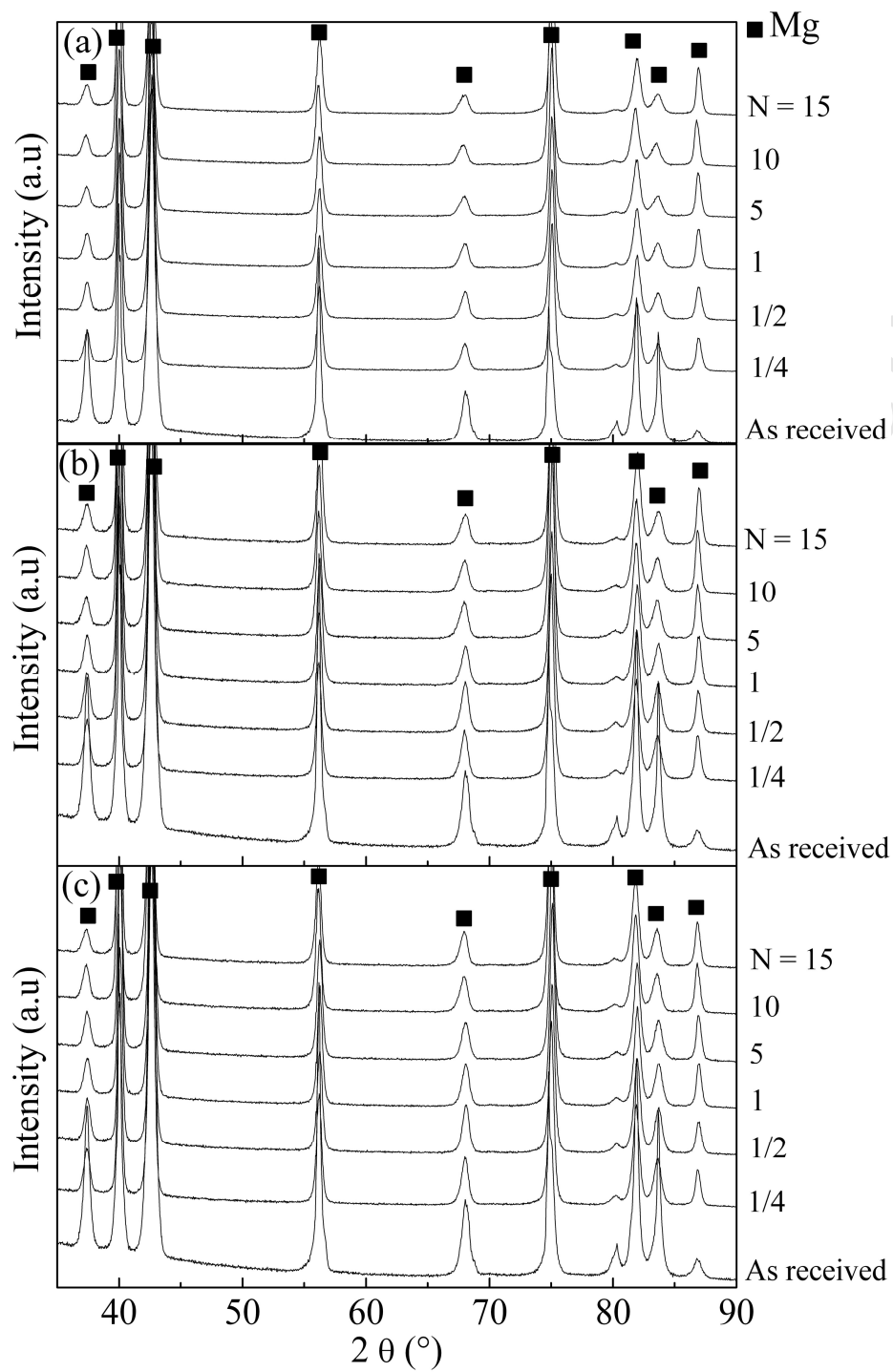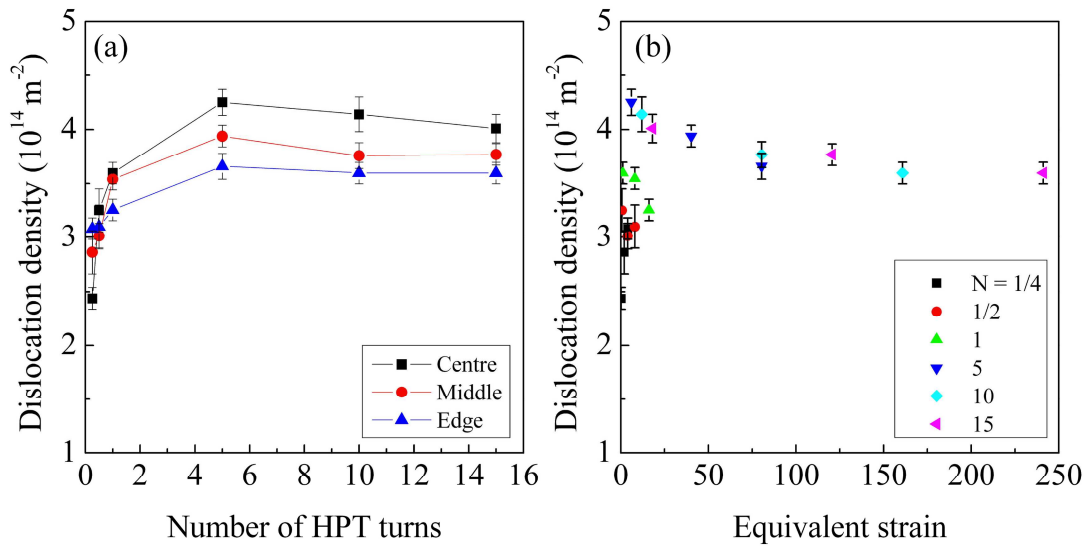
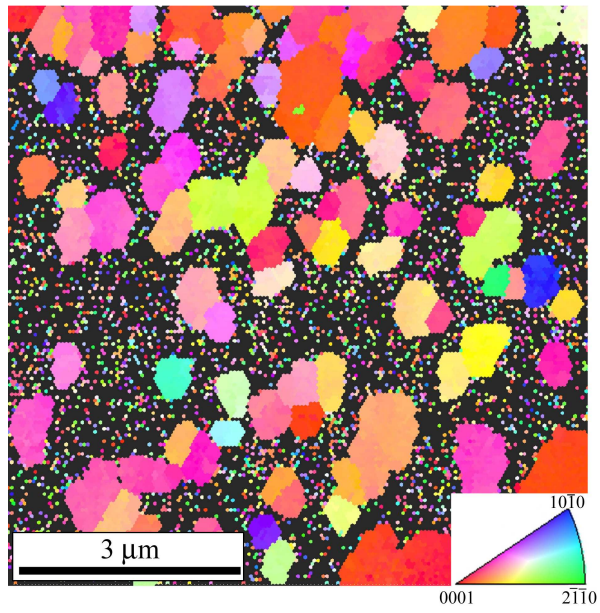**Highlights**

- A basal fiber texture is developed with some differences between the centre to edge.

- A significant grain refinement to ~0.75 μm was evident after HPT processing.

- The microstructure after 15 HPT turns contained about 77 % of recrystallized grains

- Texture strengthening makes a contribution to the rapid increase in hardening.